Report

Cell Reports

Endocardial Notch Signaling Promotes Cardiomyocyte Proliferation in the Regenerating Zebrafish Heart through Wnt Pathway Antagonism

Graphical Abstract

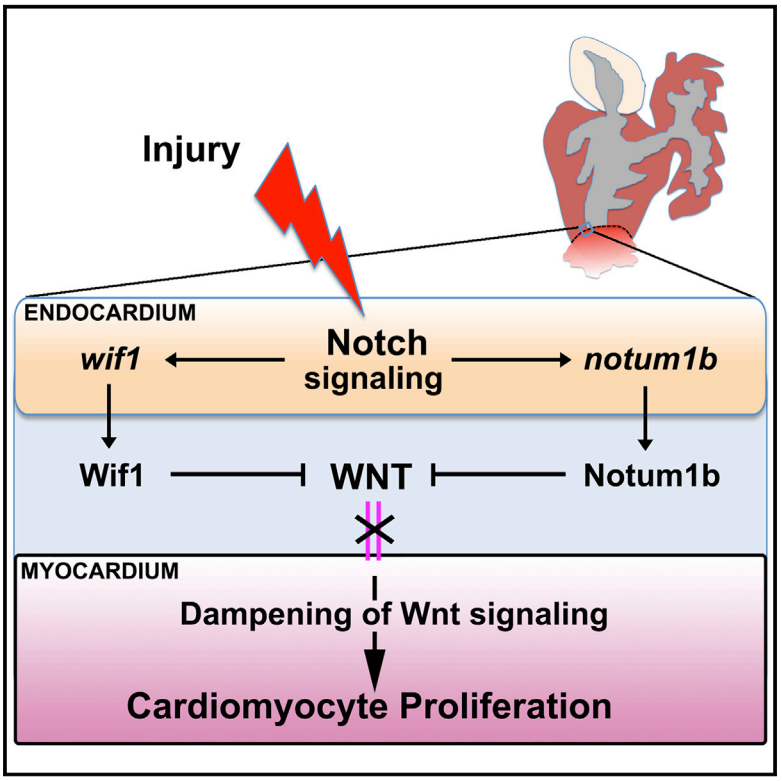

Authors

Long Zhao, Raz Ben-Yair, Caroline E. Burns, C. Geoffrey Burns

Correspondence

cburns6@mgh.harvard.edu (C.E.B.), gburns@cvrc.mgh.harvard.edu (C.G.B.)

In Brief

The highly regenerative zebrafish heart responds to injury by upregulating Notch receptors in the endocardium and epicardium to support myocardial proliferation and regeneration. Zhao et al. demonstrate that endocardial (EC) Notch signaling augments the expression of secreted endocardial Wnt antagonists that dampen myocardial Wnt signaling to support regenerative cardiomyocyte renewal.

Highlights

- EC Notch signaling is required for regenerative cardiomyocyte proliferation.
- EC Notch augments expression of secreted Wnt antagonists *notum1b* and *wif1.*
- Hyperactivated Wnt signaling suppresses regenerative cardiomyocyte proliferation.
- Wnt inhibition boosts cardiomyocyte proliferation in EC Notch-suppressed hearts.

Zhao et al., 2019, Cell Reports *26*, 546–554
January 15, 2019
https://doi.org/10.1016/j.celrep.2018.12.048

CellPress

OPEN ACCESS
CellPress

Cell Reports
Report

Endocardial Notch Signaling Promotes Cardiomyocyte Proliferation in the Regenerating Zebrafish Heart through Wnt Pathway Antagonism

Long Zhao,[1,2] Raz Ben-Yair,[1,2] Caroline E. Burns,[1,2,3,*] and C. Geoffrey Burns[1,2,4,*]
[1]Cardiovascular Research Center, Massachusetts General Hospital, Charlestown, MA 02129, USA
[2]Harvard Medical School, Boston, MA 02115, USA
[3]Harvard Stem Cell Institute, Cambridge, MA 02138, USA
[4]Lead Contact
*Correspondence: cburns6@mgh.harvard.edu (C.E.B.), gburns@cvrc.mgh.harvard.edu (C.G.B.)
https://doi.org/10.1016/j.celrep.2018.12.048

SUMMARY

Previous studies demonstrate that the regenerative zebrafish heart responds to injury by upregulating Notch receptors in the endocardium and epicardium. Moreover, global suppression of Notch activity following injury impairs cardiomyocyte proliferation and induces scarring. However, the lineage-specific requirements for Notch signaling and full array of downstream targets remain unidentified. Here, we demonstrate that inhibition of endocardial Notch signaling following ventricular amputation compromises cardiomyocyte proliferation and stimulates fibrosis. RNA sequencing uncovered reduced levels of two transcripts encoding secreted Wnt antagonists, Wif1 and Notum1b, in Notch-suppressed hearts. Like Notch receptors, *wif1* and *notum1b* are induced following injury in the endocardium and epicardium. Small-molecule-mediated activation of Wnt signaling is sufficient to impair cardiomyocyte proliferation and induce scarring. Last, Wnt pathway suppression partially restored cardiomyocyte proliferation in hearts experiencing endocardial Notch inhibition. Taken together, our data demonstrate that Notch signaling supports cardiomyocyte proliferation by dampening myocardial Wnt activity during zebrafish heart regeneration.

INTRODUCTION

Hearts of adult zebrafish and neonatal mice exhibit remarkable regenerative capacities following injury through robust cardiomyocyte proliferation (González-Rosa et al., 2017; Jopling et al., 2010; Kikuchi et al., 2010; Porrello et al., 2011; Poss et al., 2002; Raya et al., 2003). By contrast, the adult human heart is largely non-regenerative (González-Rosa et al., 2017), which reflects the naturally low cardiomyocyte turnover rate throughout adulthood (Bergmann et al., 2009, 2015). However rare, cardiomyocyte turnover does occur in adult humans, which suggests that augmenting this process in the wake of acute insult might be therapeutically beneficial. Thus, harnessing the cellular and genetic determinants that stimulate cardiomyocyte proliferation in naturally regenerative organisms might serve as an inroad for promoting heart regeneration in humans.

One such determinant in zebrafish is the Notch signaling pathway (Münch et al., 2017; Zhao et al., 2014). Notch receptors are upregulated in the endocardium (Münch et al., 2017; Raya et al., 2003; Zhao et al., 2014) and epicardium (Zhao et al., 2014) following ventricular apex amputation (Raya et al., 2003; Zhao et al., 2014) or cryoinjury (Münch et al., 2017). In both models, global suppression of Notch signaling impedes cardiomyocyte proliferation and induces scarring. Following cryoinjury, dampened myocardial proliferation was attributed to heightened inflammation and sustained endocardial expression of *serpine1* (Münch et al., 2017). Whether similar cellular and molecular mechanisms exist in the apex amputation model, where inflammation is far less prominent, remains unknown.

Aside from inflammation, endocardial Notch signaling also regulates trabeculation in mice by stimulating myocardial proliferation during embryonic development (D'Amato et al., 2016; Grego-Bessa et al., 2007; Luxán et al., 2013; VanDusen et al., 2014). Endocardial Notch signaling induces BMP10 expression in adjacent cardiomyocytes, which leads to a proliferative response (Grego-Bessa et al., 2007; Luxán et al., 2016). In zebrafish larvae, endocardial Notch signaling is required for transdifferentiation of cardiomyocytes from an atrial to ventricular fate following ventricular myocardial ablation (Zhang et al., 2013). Whether comparable tissue-specific requirements and paracrine mechanisms are active in the regenerating hearts of zebrafish remains unexplored.

Here, we report that endocardial-specific Notch inhibition dampens cardiomyocyte proliferation and leads to regenerative failures following apex amputation. Furthermore, we learned that the secreted Wnt antagonists, Wif1 and Notum1b, are significantly downregulated in Notch-suppressed hearts, suggesting that Notch-mediated Wnt pathway suppression is required to enable cardiomyocyte renewal. Accordingly, hyperactivation of Wnt signaling dampened cardiomyocyte proliferation and blocked heart regeneration. Moreover, Wnt pathway inhibition partially rescued the myocardial proliferation deficit observed in endocardial-specific Notch-suppressed hearts. Our studies provide mechanistic links between endocardial Notch activation, myocardial Wnt suppression, and the promotion of robust

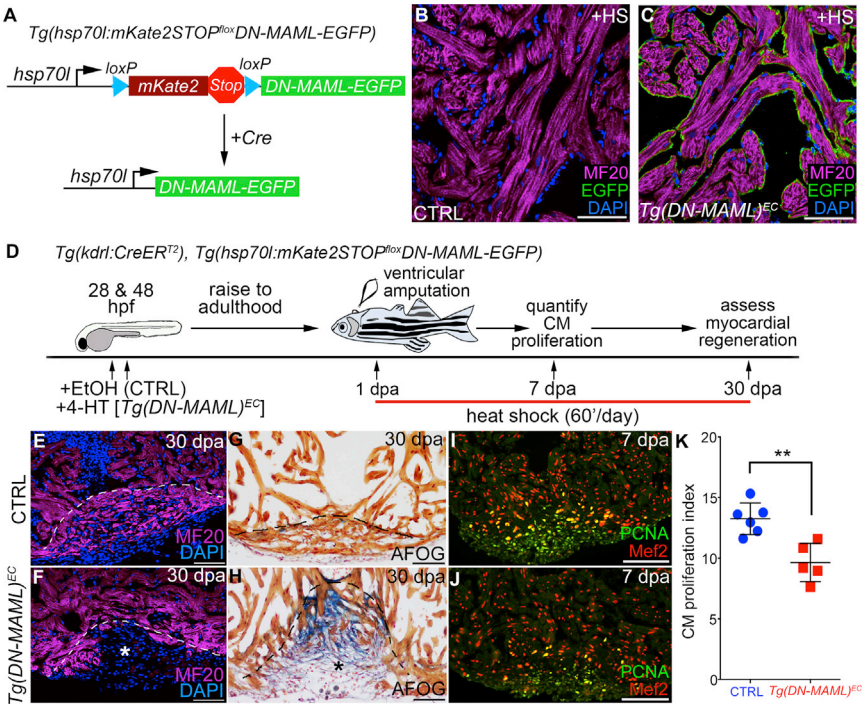

Figure 1. Endocardial Notch Signaling Is Required for Cardiomyocyte Proliferation during Zebrafish Heart Regeneration

(A) Schematic diagram of the transgene, and its Cre-dependent recombination, used to achieve tissue-specific, heat shock-inducible inhibition of Notch signaling.

(B and C) Single confocal slices of cardiac sections from *Tg(kdrl:CreER^{T2})*, *Tg(hsp70l:mKate2STOP^{flox}DN-MAML)* animals treated during embryogenesis with EtOH (CRTL) (B) or 4-HT (*Tg(hsp70l:DN-MAML)^{EC}*; abbreviated *Tg(DN-MAML)^{EC}*) (C), raised to adulthood, heat shocked once, and sacrificed 5 hr later for analysis. Sections were double immunostained for MF20 (magenta) and GFP (green) and counterstained with DAPI (blue). Greater than three sections from more than 5 hearts per group were examined. Little to no variation was observed.

(D) Double-transgenic strain and experimental strategy employed to inhibit Notch signaling specifically in endocardial cells during zebrafish heart regeneration.

(E–J) Cardiac sections from *kdrl:CreER^{T2}*, *hsp70l:mKate2STOP^{flox}DN-MAML* animals treated during embryogenesis with EtOH (CRTL) (E, G, and I) or 4-HT (*Tg(hsp70l:DN-MAML^{EC})*; abbreviated *Tg(DN-MAML)^{EC}*) (F, H, and J), raised to adulthood, subjected to ventricular apex amputation, and heat shocked daily.

(E and F) Single confocal slices of cardiac sections from 30 days post-amputation (dpa) animals immunostained for MF20 (magenta) and counterstained with DAPI (blue). Dashed lines approximate the amputation planes. The asterisk in (F) highlights a gap in the myocardial wall.

(G and H) Cardiac sections from 30 dpa animals stained with AFOG to detect muscle (brown), fibrin (red), and collagen (blue). The asterisk in (H) highlights collagen-rich scar tissue (H). Myocardial regeneration occurred in 10/10 CTRL and 1/16 *Tg(DN-MAML)^{EC}* hearts.

(I and J) Compound microscopic images of cardiac sections from 7 dpa CTRL and *Tg(DN-MAML)^{EC}* animals double immunostained to detect cardiomyocyte nuclei (α-Mef2 antibody; red) and cycling cells (α-PCNA antibody; green).

(K) Bar graph showing cardiomyocyte proliferation indices on 7 dpa in CTRL (n = 6) and *Tg(DM-MAML)^{EC}* (n = 5) hearts. Proliferation data were collected for 4–6 sections per heart and averaged to generate each data point. Statistical significance was determined using a Student's t test. Error bars: ±1 SD. **$p < 0.01$. Scale bars: 50 μm.

cardiomyocyte proliferation in the wake of acute cardiac injury in zebrafish.

RESULTS

Endocardial Notch Signaling Is Required for Zebrafish Heart Regeneration by Supporting Cardiomyocyte Proliferation

To understand the lineage-specific requirements for Notch signaling in zebrafish heart regeneration, we evaluated the consequences of endocardial-specific Notch inhibition following cardiac injury. To achieve tissue-specific, inducible suppression of Notch signaling, we created a conditional transgene that can be recombined by Cre recombinase to express a GFP-tagged version of the previously validated (Zhao et al., 2014) murine Notch inhibitor DN-MAML (dominant-negative mastermind like) from the zebrafish heat shock promoter (Figure 1A). In addition, we employed the previously validated *kdrl:CreER^{T2}* driver line (Harrison et al., 2015; Zhao et al., 2014), which expresses 4-hydroxytamoxifen (4-HT)-inducible Cre recombinase in endothelial/endocardial cells (Jin et al., 2005; Zhao et al., 2014). To validate the system, we exposed double-transgenic embryos to EtOH or 4-HT between 20 hr post-fertilization (hpf) and 40 hpf, heat shocked the animals once at 45 hpf, and fixed them for immunostaining with a GFP antibody 5 hr later. Embryos exposed to EtOH were devoid of GFP expression (Figures S1A–S1B′), whereas those treated with 4-HT displayed GFP expression in endocardial and endothelial cells (Figures S1C–S1D′). To confirm that heat shock inducibility of DN-MAML persisted into adulthood, we raised EtOH- and 4-HT-treated (*Tg(hsp70l:DN-MAML)$^{Endocardial\ Cell}$*; abbreviated *Tg(DN-MAML)^{EC}*) animals to 6 months of age, heat shocked again, and examined cardiac sections immunostained for GFP. Only those animals treated with 4-HT during embryogenesis displayed GFP expression specifically in the endocardium of the adult heart (Figures 1B and 1C).

Next, we performed ventricular apex amputations on control and *Tg(DN-MAML)^{EC}* zebrafish at approximately 6 months of age (Figure 1D). Injured animals were heat shocked daily for 1 hr over the course of 30 days to inhibit Notch signaling in endothelial/endocardial cells during the regenerative window. Thereafter, we examined cardiac sections immunostained with the myocardial-specific MF20 antibody. We also quantified scar size in sections stained with Acid Fuschin-Orange G (AFOG). While control hearts consistently contained regenerated muscle and minimal fibrosis (Figures 1E, 1G, S1E–H, S1M–S1P,

and S1U), *Tg(DN-MAML)*^{EC} hearts displayed myocardial deficits (Figures 1F and S1I–S1L) and prominent scar tissue where the ventricle was wounded (Figures 1H and S1Q–S1U).

Because heat shocking *Tg(DN-MAML)*^{EC} animals induces DN-MAML expression not only in the endocardium, but also in vascular endothelial cells (Figures S1C–S1D′), we evaluated injured and heat-shocked *Tg(DN-MAML)*^{EC} animals for coronary artery abnormalities (Figure S2A–S2H′) and for evidence of surface bleeding (Figure S2I–S2S) to predict the likelihood that a vessel defect might contribute to the regenerative failures. However, no phenotypes were observed, thereby minimizing the likelihood that endothelial Notch inhibition contributes to the regenerative deficiencies.

New heart muscle derives from cardiomyocytes along the wound edge that undergo proliferative expansion (Jopling et al., 2010; Kikuchi et al., 2010). Because global Notch inhibition suppresses cardiomyocyte proliferation (Münch et al., 2017; Zhao et al., 2014), we tested whether endocardial-specific Notch inhibition similarly impairs cardiomyocyte renewal. We compared the percentages of wound edge cardiomyocytes expressing the DNA replication marker PCNA in heat-shocked control and *Tg(DN-MAML)*^{EC} animals on 7 days post-amputation (dpa) (Figure 1D) and observed a 27% reduction in the proliferative index (Figures 1I–1K). Together, these data indicate that endocardial Notch signaling performs non-cell-autonomous role in myocardial regeneration by promoting cardiomyocyte proliferation, likely by stimulating the production of a paracrine signal.

Injury-Induced Notch Signaling Regulates Expression of Transcripts Encoding the Secreted Wnt Antagonists, Wif1 and Notum1b

To identify candidate signals, we performed RNA sequencing on wound edge tissue collected from wild-type animals and those induced to express DN-MAML globally (i.e., *Tg(hsp70l:DN-MAML)*^{ubiquitous}; abbreviated *Tg(DN-MAML)*^{ubi}) (Zhao et al., 2014). After daily heat shocking of both groups following injury, we performed expression profiling on 5 dpa, which corresponds to early cardiomyocyte proliferation (Poss et al., 2002). Using a strict significance threshold ($p < 0.0001$), we identified 131 downregulated and 123 upregulated transcripts in Notch-suppressed hearts (Figures 2A and S3A; Table S1). Consistent with the non-regenerative nature of heat-shocked *Tg(DN-MAML)*^{ubi} hearts (Zhao et al., 2014), gene ontology (GO) enrichment analysis identified "mitosis," "cell cycle," and "chromosome segregation" categories as overrepresented in the downregulated gene cluster (Figures 2B and S3B). We surveyed the list of downregulated genes to identify secreted factors whose production relies on Notch signaling (Figures S3A and S3C; Table S1) and were intrigued to find transcripts encoding the secreted Wnt antagonists Wif1 and Notum1b (Figures 2C, S3A, and S3C; Table S1). Using qPCR, we confirmed significant declines in *wif1* and *notum1b* expression when Notch signaling is globally suppressed (Figure 2D).

To learn whether *wif1* and *notum1b* are normally upregulated by cardiac injury, we compared their expression levels between uninjured and 7 dpa hearts from wild-type animals and observed ~1.4-fold increases of each following injury (Figure 2E). Using *in situ* hybridization, we learned that both transcripts appear scattered in the endocardium (Figures 2F, 2F′, 2G, and 2G′) and are more prominent in the epicardium covering the wound (Figures 2F and 2G), a pattern reminiscent of Notch receptor expression (Münch et al., 2017; Raya et al., 2003; Zhao et al., 2014). To achieve increased sensitivity, we immunostained 7 dpa cardiac sections with commercially available antibodies predicted to recognize Wif1 and Notum1b. In both cases, prominent staining was observed adjacent to the ventricular myocardium (Figures 2H–2I′) in what we confirmed to be endocardial cells through colocalization with a transgenic reporter (Figures S4A–S4B″). In addition, we observed significant overlap between each Wnt antagonist and pan-cytokeratin+ (PCK+) epicardial cells both proximal (Figures S4H–S4H″ and S4J–S4J″) and distal (Figures S4I–S4I″ and S4K–S4K″) to the wound. Last, we learned that neither protein is co-expressed with collagen, type I, alpha 1 (Col1a1) (Figures S4L–S4M‴), which marks wound fibroblasts (González-Rosa et al., 2012). Overall, these data demonstrate that endocardial and epicardial cells, but not fibroblasts, are sources of Wif1 and Notum1b during zebrafish heart regeneration.

Because we identified *wif1* and *notum1b* as downregulated transcripts in hearts experiencing global Notch suppression (Figures 2A–2D), we sought to determine whether endocardial-specific Notch inhibition also lowers *wif1* and *notum1b* levels and, if so, whether this decrease occurs preferentially in the endocardium. We used qPCR to compare the relative expression levels of *wif1* and *notum1b* between 5 dpa control and *Tg(DN-MAML)*^{EC} animals in two regions of the injured ventricle that contain proportionally more epicardium or endocardium (Figure S5A). Specifically, we analyzed gene expression in the epicardium-enriched wound or the tissue adjacent to the amputation plane, which contains relatively more endocardium. We observed significant declines in *wif1* and *notum1b* levels exclusively in the tissue adjacent to the wound (Figures S5B and S5C). Therefore, like global Notch pathway suppression (Figures 2C and 2D), endocardial-specific Notch pathway inhibition also results in significant decreases in *wif1* and *notum1b* levels (Figures S5A–S5C), which is likely confined to the endocardium of the heart.

Inhibition of Notch Signaling Augments Myocardial Wnt Signaling following Cardiac Injury

A previous report demonstrated that Wnt signaling activity, as monitored by a transgenic reporter, is observed at the wound edge in regenerating zebrafish hearts (Stoick-Cooper et al., 2007). To gain lineage resolution, we analyzed injured hearts from the independent Wnt reporter strain *Tg(7XTCF:eGFP)* (Moro et al., 2012). Cardiac sections from 5 dpa animals were double immunostained for GFP and the myocardial-specific MF20 antibody (Figures 3A and 3C–3C″). We corroborated the previous report that Wnt signaling is detectable near the wound edge (Stoick-Cooper et al., 2007) and learned that signaling is evident preferentially in the myocardium (Figures 3A and 3C–3C″).

Considering that cardiac injury stimulates Notch-dependent expression of two Wnt antagonists, we hypothesized that Wnt signaling might be augmented by global Notch pathway suppression. We treated *Tg(7XTCF:eGFP)* fish daily with the Notch antagonist N-[N-(3,5-Difluorophenacetyl)-L-alanyl]-S-phenylglycine

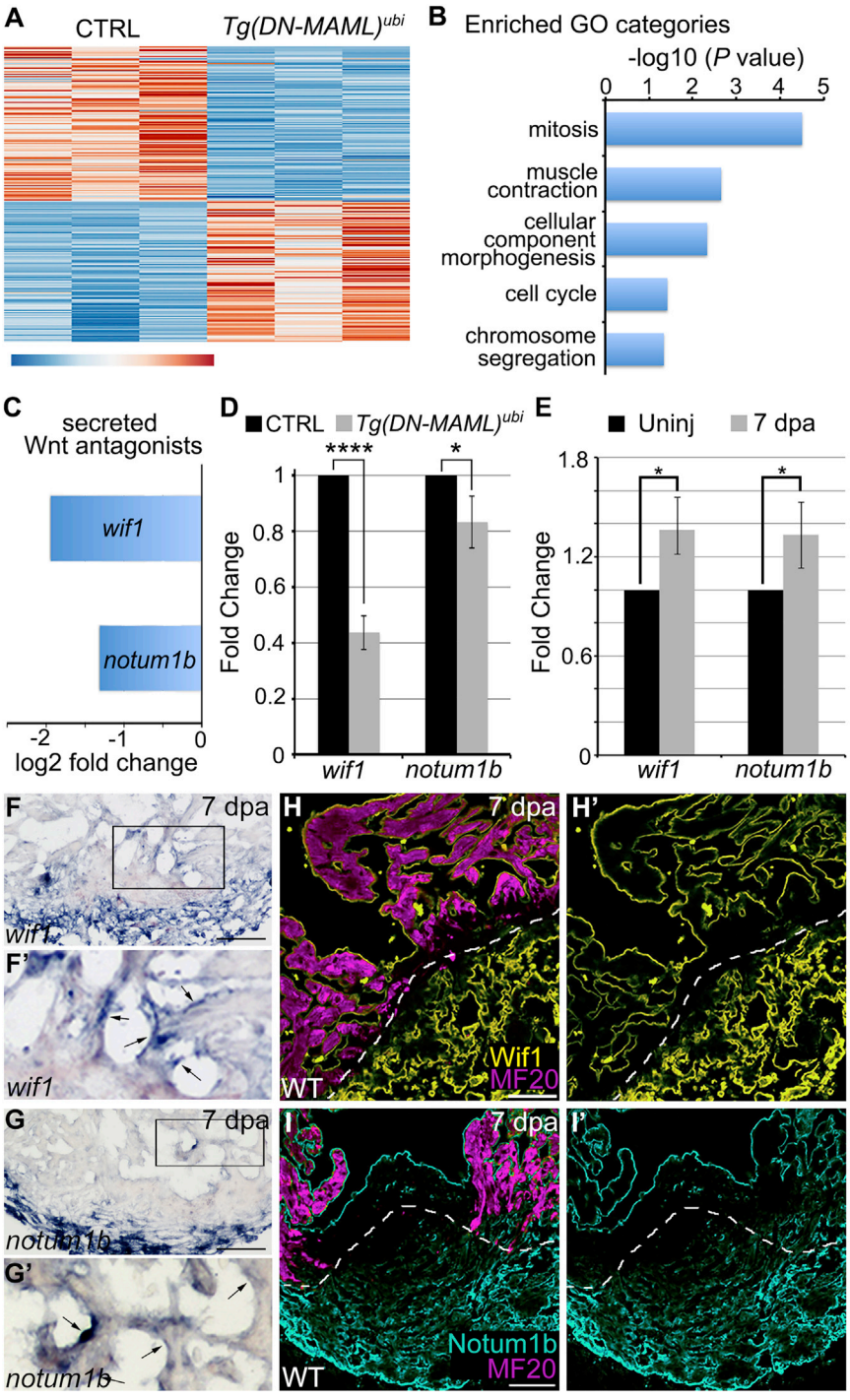

Figure 2. Identification of Secreted Wnt Signaling Antagonists as Candidate Notch Targets in the Endocardium during Zebrafish Heart Regeneration

(A) Heatmap showing 254 differentially expressed genes ($p < 0.0001$) in wild-type (CTRL; n = 3 replicates) and *Tg(hsp70l:DN-MAML)* (n = 3 replicates) hearts on 5 dpa with daily heat shocking.

(B) Bar graph showing −log10 p values for GO terms significantly overrepresented in the down-regulated gene category.

(C) Bar graph showing the log2 fold-change values for transcripts encoding *wif1* and *notum1b* from (A).

(D) Bar graph showing the relative expression levels of *wif1* and *notum1b* in hearts of CTRL and *hsp70l:DN-MAML* animals on 5 dpa with daily heat shocking as measured by qPCR.

(E) Bar graph showing the relative expression levels of *wif1* and *notum1b* in hearts of wild-type animals without injury and on 7 dpa as measured by qPCR.

(D and E) 3 technical replicates of each of 3 biological replicates were performed. Statistical significance was determined using a Student's t test. Error bars: ±1 SD. ****$p < 0.0001$. *$p < 0.05$.

(F–G′) *In situ* hybridization for *wif1* and *notum1b* in cardiac sections of wild-type hearts on 7 dpa. Boxed regions in (F) and (G) are enlarged in (F′) and (G′). Arrowheads highlight endocardial signals. 6–8 sections from 4–6 hearts were analyzed. Little to no variation was observed.

(H–I′) Immunohistochemical analysis of Wif1 (H and H′; yellow) and Notum (I and I′; cyan) in cardiac sections of wild-type hearts on 7 dpa costained with the MF20 antibody (magenta) to visualize myocardium. Single confocal slices are shown. Dashed lines highlight approximate amputation planes. 6–8 sections from 4–6 hearts were analyzed. Little to no variation was observed. Scale bars: 50 μm.

t-butyl ester (DAPT) and compared the brightness and distribution of GFP fluorescence to that observed in DMSO-treated hearts. Although GFP remained localized to the myocardium, levels were qualitatively higher and broader in Notch-inhibited hearts (Figures 3A–3D″), demonstrating that Notch signaling tempers myocardial Wnt pathway activation during the regenerative window.

To evaluate Wnt signaling in hearts with endocardial Notch inhibition, we used qPCR to measure the relative abundances of three previously validated Wnt targets in 5 dpa control and *Tg(DN-MAML)^{EC}* hearts. While one target, *mycn* (Alexander et al., 2014), showed highly variable expression between replicates, the other two targets, *axin2* (Alexander et al., 2014) and *ccnd1* (Nery et al., 2014), were found to be significantly increased in injured *Tg(DN-MAML)^{EC}* hearts (Figure S6A), suggesting that endocardial Notch signaling functions to restrain Wnt signaling during heart regeneration.

Suppression of Wnt Signaling Is Required for Zebrafish Heart Regeneration

Because cardiac injury stimulates expression of Wnt antagonists and a blunting of this response in Notch-inhibited animals

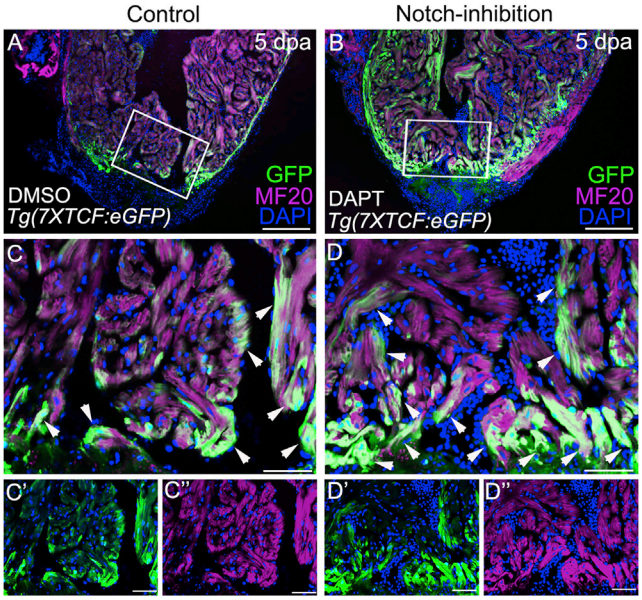

Figure 3. Notch Inhibition Boosts Wnt Signaling in the Myocardium of Injured Zebrafish Hearts

(A and B) Confocal slices of cardiac sections from 5 dpa *Tg(7xTCF:eGFP)* animals injected daily with DMSO (A) or N-[N-(3,5-Difluorophenacetyl)-L-alanyl]-S-phenylglycine t-butyl ester (DAPT) (B). Animals were double immunostained to detect GFP (green) and myocardium (MF20 antibody; magenta) and counterstained with DAPI (blue).

(C–D″) Boxed regions in (A) and (B) are shown at higher magnification in (C) and (D). Split channels are shown in (C′), (C″), (D′), and (D″). Arrows point to myocardial cells with active Wnt signaling. n = 3 hearts per experimental group. At least 3 sections were examined per heart. Little to no variability was observed between animals in each experimental group.

is associated with regenerative failures, we hypothesized that Wnt pathway suppression might be a natural requirement for myocardial regeneration in zebrafish. Therefore, we modulated Wnt activity following injury in wild-type animals using the small-molecule antagonist IWR-1-endo (IWR) (Chen et al., 2009; Huang et al., 2009) or agonist 6-bromoindirubin-3-oxime (BIO) (Polychronopoulos et al., 2004; Sato et al., 2004). Injections of IWR or BIO into uninjured animals caused *axin2*, *ccnd1*, and *mycn* levels to drop or increase, respectively, by approximately 50% (Figure S6B), which validates the use of these small molecules to modulate Wnt signaling during regeneration.

We performed ventricular apex resection and injected injured animals with vehicle (DMSO), IWR, or BIO every other day for 30 days (Figure 4A). Cardiac sections were stained with MF20 or AFOG to assess myocardial renewal and fibrosis, respectively. While the majority of DMSO-treated (87.5%; Figures 4B, 4E, S6C–F, S6O–S6R, and S6AA) and Wnt-inhibited (IWR treated; 57%; Figures 4C, 4F, S6G–S6J, S6S–S6V, and S6AA) hearts contained regenerated segments of muscle with minimal fibrosis, 75% of those with augmented Wnt signaling (BIO treated; Figures 4D, 4G, S6K–S6N, and S6W–S6AA) failed to regenerate as evidenced by discontinuities in the myocardial wall (Figure 5D) that were filled with fibrin and collagen (Figure 4G). Thus, hyperactivating Wnt signaling in the wake of cardiac injury creates an impediment to myocardial renewal and is consistent with the notion that Wnt signaling must be lowered to enable natural heart regeneration.

Next, we injured wild-type animals and injected them with DMSO, IWR, or BIO on 5 and 6 dpa before quantifying cardiomyocyte proliferation on 7 dpa (Figure 4A). Remarkably, we learned that the inhibition of Wnt signaling is sufficient to increase cardiomyocyte proliferation (Figures 4H–4I′ and 4K), demonstrating that endogenous Wnt signaling naturally tempers the pace at which cardiomyocytes are produced during regeneration. By contrast, Wnt hyperactivation reduced myocardial proliferation by 42% (Figures 4H, 4H′, 4J, 4J′, and 4K), consistent with the lack of regeneration observed at 30 dpa (Figures 4D, 4G, S6K–S6N, and S6W–S6AA). Together, these data demonstrate that suppression of Wnt signaling is necessary and sufficient to drive cardiomyocyte proliferation during zebrafish heart regeneration.

Suppressing Wnt Signaling in *Tg(DN-MAML)^{EC}* Animals Partially Rescues Cardiomyocyte Proliferation

Next, we tested the hypothesis that attenuating Wnt signaling in heat-shocked *Tg(DN-MAML)^{EC}* animals would rescue their cardiomyocyte proliferation deficit (Figures 1I–1K). We resected the ventricular apices of control and *Tg(DN-MAML)^{EC}* zebrafish and exposed them to daily heat shock from 1 to 7 dpa (Figure 5A). On 5 and 6 dpa, animals were injected intraperitoneally with DMSO or the Wnt antagonist and wound edge cardiomyocyte proliferation was quantified on 7 dpa (Figure 5A). Consistent with previous experiments (Figures 1I–1K, 4H–4I′, and 4K), wild-type animals treated with IWR and *Tg(DN-MAML)^{EC}* animals treated with DMSO exhibited augmented (Figures 5B–5C′ and 5F) and restrained (Figures 5B, 5B′, 5D, 5D′, and 5F) cardiomyocyte proliferation, respectively. Consistent with our hypothesis, suppression of Wnt signaling in *Tg(DN-MAML)^{EC}* animals boosted cardiomyocyte proliferation by 44%, from 7.65% to 11.03% (Figures 5E, 5E′, and 5F), which represents a partial phenotypic rescue. Although the combination of prolonged heat shocking with small-molecule treatments proved too toxic to assess myocardial regeneration at 30 dpa, our data support a model in which myocardial Wnt signaling functions as a negative regulator of myocardial proliferation downstream of endocardial Notch signaling during zebrafish heart regeneration (Figure 5G).

DISCUSSION

We demonstrate that endocardial Notch signaling is required for heart regeneration in zebrafish and identify the secreted Wnt antagonists, Wif1 and Notum1b, as downstream targets of Notch signaling in this context. Whether Notch is also required in the epicardium remains to be tested. Although Wif1 and Notum1b both function extracellularly to inhibit Wnt signaling, they do so through different mechanisms. Specifically, Wif1 binds directly to Wnt ligands to prevent their interaction with cell surface receptors (Hsieh et al., 1999), while Notum1b is a carboxylesterase that renders Wnt ligands inactive (Kakugawa et al., 2015). This

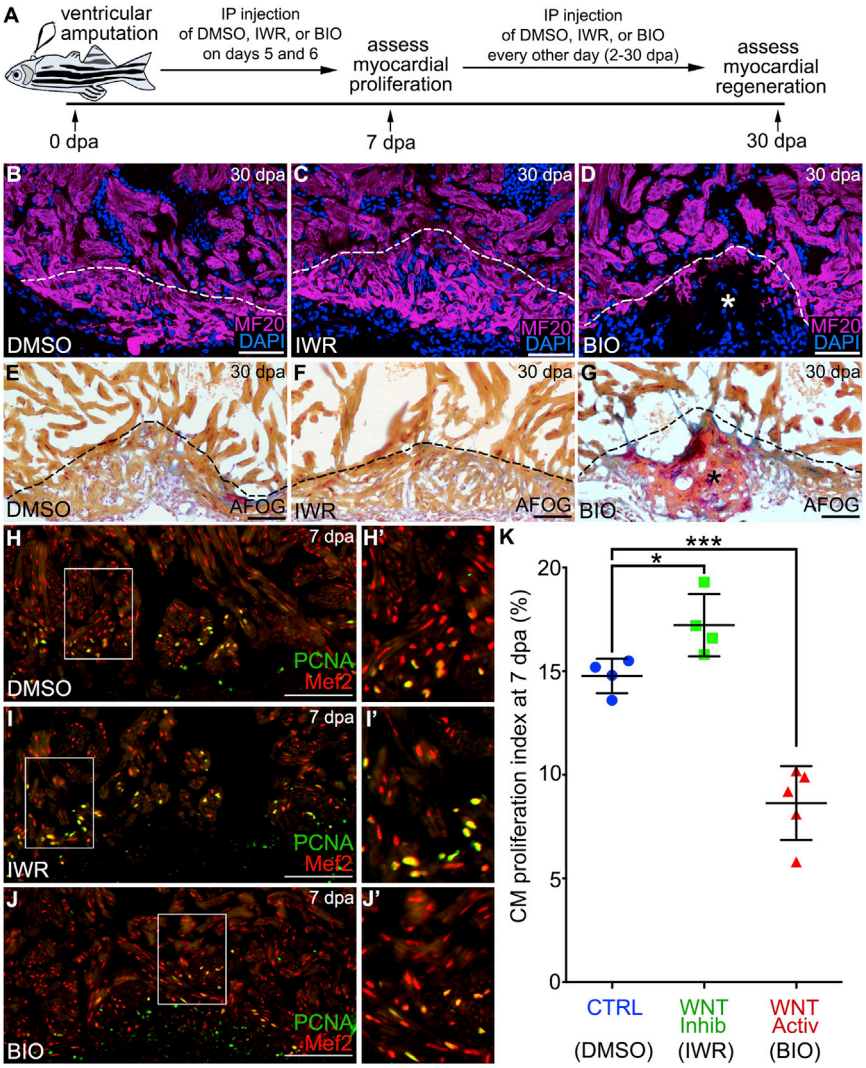

Figure 4. Inhibition of Wnt Signaling Is Required for Zebrafish Heart Regeneration by Bolstering Myocardial Proliferation

(A) Experimental strategy used to inhibit or augment Wnt signaling during the regenerative window. Injured animals were injected intraperitoneally (IP) with DMSO, IWR, or BIO on 5 and 6 dpa before cardiomyocyte proliferation was measured on 7 dpa. Myocardial regeneration was examined on 30 dpa followed by IP injection of DMSO, IWR, or BIO every other day throughout 2–30 dpa.

(B–G) Cardiac sections from 30 dpa wild-type animals injected with DMSO (B and E), IWR (C and F), or BIO (D and G). Single confocal slices of sections immunostained with MF20 (magenta) and counterstained with DAPI (blue) are shown in (B)–(D). Sections stained with AFOG to visualize muscle (brown), fibrin (red), and collagen (blue) are shown in (E)–(G). Asterisks in (D) and (G) highlight gaps in the myocardial wall filled with collagen-rich scar tissue. Heart regeneration occurred in 7/8 DMSO-treated, 4/7 IWR-treated, and 2/8 BIO-treated animals.

(H–J′) Cardiac sections from 7 day post-amputation wild-type animals treated with DMSO (H and H′), IWR (I and I′), and BIO (J and J′) were double immunostained to detect cardiomyocyte nuclei (Mef2 antibody; red) and cycling cells (α-PCNA antibody; green). Compound microscopic images are shown.

(K) Bar graph showing cardiomyocyte proliferation indices for the indicated experimental groups (DMSO, n = 4; IWR, n = 4; BIO, n = 5). 4–6 sections per heart were analyzed and averaged to generate each data point. Statistical significance was determined using a Student's t test. Error bars: ±1 SD. *$p < 0.05$. ***$p < 0.001$. Scale bars: 50 μm.

type of multimodal repressive mechanism suggests that injury-induced cardiomyocyte proliferation requires fine-tuning of Wnt activity, which is controlled at least in part by endocardial Notch signaling.

Precedence for this type of antagonistic cross talk between the Notch and Wnt pathways exists in other biological contexts where the balance between cellular proliferation and differentiation is tightly regulated (Boulter et al., 2012; Gu et al., 2013; Huang et al., 2014; Kwon et al., 2011; Li et al., 2015; Nicolas et al., 2003; Tian et al., 2015). For example, Notch signaling in mouse intestinal stem cells dampens Wnt activity to maintain the progenitor pool (Tian et al., 2015). In the mouse epidermis, Notch signaling also represses Wnt, but in this case to maintain the differentiated keratinocyte fate (Nicolas et al., 2003). Although heart regeneration occurs primarily through a stem cell-independent mechanism (González-Rosa et al., 2017; Jopling et al., 2010; Kikuchi et al., 2010; Porrello et al., 2011), our data suggest that opposing Notch and Wnt signals might balance the proportion of proliferating and working cardiomyocytes to promote effective organ renewal while simultaneously sustaining cardiac output, respectively.

The influence of Wnt signaling on cardiomyocyte proliferation appears to be context dependent. While studies employing cultured rat cardiomyocytes and embryonic mice have demonstrated that Wnt/β-catenin signaling is a positive regulator of cardiomyocyte proliferation in the absence of insult (Buikema et al., 2013; Heallen et al., 2011; Ozhan and Weidinger, 2015; Tseng et al., 2006; Ye et al., 2015), our data have uncovered an injury-dependent inhibitory role during zebrafish heart regeneration. This function is likely to be conserved in mammals as inhibition of Wnt signaling following experimental myocardial infarction in mice stimulated cardiomyocyte proliferation and improved outcomes (Bastakoty et al., 2016; Yang et al., 2017).

Overall, our findings reinforce the importance of endocardial-myocardial cross talk during zebrafish heart regeneration (Kikuchi et al., 2011) and highlight a potential inroad for therapeutic intervention. Interestingly, transgenic mice harboring a fluorescent Notch reporter showed strong upregulation of Notch activity in the endocardium and epicardium following induced

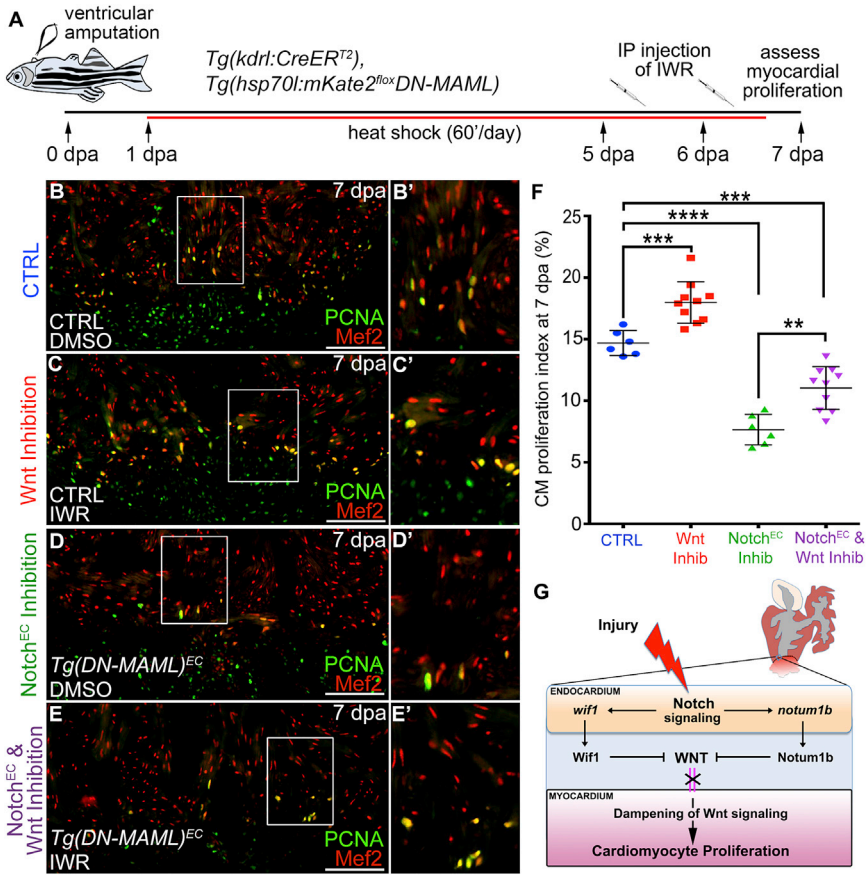

Figure 5. Wnt Inhibition Partially Rescues Cardiomyocyte Proliferation Deficits Caused by Impaired Endocardial Notch Signaling

(A) Double-transgenic strain and schematic diagram of experimental timeline used to inhibit Wnt signaling in animals with compromised endocardial Notch signaling.

(B–E′) Compound microscopic images of cardiac sections from *kdrl:CreER*^{T2}*; hsp70l:mKate2STOP*^{flox}*DN-MAML* animals treated during embryogenesis with EtOH (CTRL) (B–C′) or 4-HT (*hsp70l:DN-MAML*^{EC}) (D–E′), raised to adulthood, and subjected to ventricular apex amputation. Thereafter, animals were heat shocked daily and treated with DMSO (B, B′, D, and D′) or the Wnt inhibitor IWR-1 (C, C′, E, and E′) before cardiomyocyte proliferation analysis on 7 dpa. Sections were double immunostained to detect cardiomyocyte nuclei (Mef2 antibody; red) and cycling cells (PCNA antibody; green). Boxed regions in (B), (C), (D), and (E) are enlarged in (B′), (C′), (D′), and (E′).

(F) Bar graph showing the cardiomyocyte proliferation indices for the indicated experimental groups (CTRL, n = 6; Wnt Inhib, n = 10; Notch^{EC} Inhib, n = 6; Notch^{EC} and Wnt Inhib, n = 10). 4–6 sections per heart were analyzed and averaged to generate each data point. Statistical significance was determined using a Student's t test. Error bars: ±1 SD. ***p < 0.001. ****p < 0.0001. **p < 0.01. Scale bars: 50 μm.

(G) Schematic diagram showing the influence of endocardial Notch on Wnt signaling and cardiomyocyte proliferation.

myocardial infarction (Russell et al., 2011). Although the adult mammalian heart ultimately becomes fibrotic, it might be possible to repurpose this natural injury response to stimulate myocardial proliferation instead of scarring.

STAR★METHODS

Detailed methods are provided in the online version of this paper and include the following:

- KEY RESOURCES TABLE
- CONTACT FOR REAGENT AND RESOURCE SHARING
- EXPERIMENTAL MODEL AND SUBJECT DETAILS
- METHOD DETAILS
  - Construction of Tg(hsp70l:mKate2STOP^{flox}DN-MAML) Transgenic Line
  - 4-HT treatments and heat shock induction
  - Histological analysis and imaging
  - Quantification of Scar Tissue in Regenerated Hearts
  - Alkaline phosphatase staining
  - Quantification of vessel leakiness
  - RNA sequencing and transcriptomic analysis
  - Small molecule treatments
  - Quantitative PCR
- QUANTIFICATION AND STATISTICAL ANALYSIS
- DATA AND SOFTWARE AVAILABILITY

SUPPLEMENTAL INFORMATION

Supplemental Information includes six figures and two tables and can be found with this article online at https://doi.org/10.1016/j.celrep.2018.12.048.

ACKNOWLEDGMENTS

We thank L. Pantano of the Harvard Chan Bioinformatics Core, Harvard T.H. Chan School of Public Health (Boston, MA), who was supported by funds from the Harvard Stem Cell Institute Center for Stem Cell Bioinformatics, for assistance with the transcriptomics analysis. We thank N. Chi for providing the *Tg(kdrl:mCherry-ras)*^{s896} strain. We thank S. Grainger and D. Traver for providing adult *Tg(7XTCF:eGFP)*^{ia4} Wnt reporter fish. L.Z. was supported by an American Heart Association postdoctoral fellowship (14POST20380738). R.B.-Y. was supported by a European Molecular Biology Organization (EMBO) long-term fellowship (LTF 119-2012). This work was supported by NIH award R01 HL127067 and Hassenfeld awards to C.G.B. and C.E.B. and by NIH R35 HL135831 and d'Arbeloff MGH Research Scholar awards to C.E.B.

AUTHOR CONTRIBUTIONS

L.Z. designed, performed, and interpreted the majority of experiments. R.B.-Y. assisted with dissection of ventricular apices and RNA isolation for RNA sequencing. L.Z., C.E.B., and C.G.B. conceived the study, designed experiments, interpreted data, and wrote the manuscript with input from all authors.

DECLARATION OF INTERESTS

The authors declare no competing interests.

Received: April 6, 2018
Revised: November 7, 2018
Accepted: December 11, 2018
Published: January 15, 2019

REFERENCES

Alexander, C., Piloto, S., Le Pabic, P., and Schilling, T.F. (2014). Wnt signaling interacts with bmp and edn1 to regulate dorsal-ventral patterning and growth of the craniofacial skeleton. PLoS Genet. *10*, e1004479.

Bastakoty, D., Saraswati, S., Joshi, P., Atkinson, J., Feoktistov, I., Liu, J., Harris, J.L., and Young, P.P. (2016). Temporary, systemic inhibition of the WNT/β-catenin pathway promotes regenerative cardiac repair following myocardial infarct. Cell Stem Cells Regen. Med. *2*, 10.16966/2472-6990.111.

Bergmann, O., Bhardwaj, R.D., Bernard, S., Zdunek, S., Barnabé-Heider, F., Walsh, S., Zupicich, J., Alkass, K., Buchholz, B.A., Druid, H., et al. (2009). Evidence for cardiomyocyte renewal in humans. Science *324*, 98–102.

Bergmann, O., Zdunek, S., Felker, A., Salehpour, M., Alkass, K., Bernard, S., Sjostrom, S.L., Szewczykowska, M., Jackowska, T., Dos Remedios, C., et al. (2015). Dynamics of cell generation and turnover in the human heart. Cell *161*, 1566–1575.

Boulter, L., Govaere, O., Bird, T.G., Radulescu, S., Ramachandran, P., Pellicoro, A., Ridgway, R.A., Seo, S.S., Spee, B., Van Rooijen, N., et al. (2012). Macrophage-derived Wnt opposes Notch signaling to specify hepatic progenitor cell fate in chronic liver disease. Nat. Med. *18*, 572–579.

Buikema, J.W., Mady, A.S., Mittal, N.V., Atmanli, A., Caron, L., Doevendans, P.A., Sluijter, J.P.G., and Domian, I.J. (2013). Wnt/β-catenin signaling directs the regional expansion of first and second heart field-derived ventricular cardiomyocytes. Development *140*, 4165–4176.

Chablais, F., Veit, J., Rainer, G., and Jaźwińska, A. (2011). The zebrafish heart regenerates after cryoinjury-induced myocardial infarction. BMC Dev. Biol. *11*, 21.

Chen, B., Dodge, M.E., Tang, W., Lu, J., Ma, Z., Fan, C.-W., Wei, S., Hao, W., Kilgore, J., Williams, N.S., et al. (2009). Small molecule-mediated disruption of Wnt-dependent signaling in tissue regeneration and cancer. Nat. Chem. Biol. *5*, 100–107.

Chi, N.C., Shaw, R.M., De Val, S., Kang, G., Jan, L.Y., Black, B.L., and Stainier, D.Y.R. (2008). Foxn4 directly regulates tbx2b expression and atrioventricular canal formation. Genes Dev. *22*, 734–739.

D'Amato, G., Luxán, G., del Monte-Nieto, G., Martínez-Poveda, B., Torroja, C., Walter, W., Bochter, M.S., Benedito, R., Cole, S., Martinez, F., et al. (2016). Sequential Notch activation regulates ventricular chamber development. Nat. Cell Biol. *18*, 7–20.

González-Rosa, J.M., Peralta, M., and Mercader, N. (2012). Pan-epicardial lineage tracing reveals that epicardium derived cells give rise to myofibroblasts and perivascular cells during zebrafish heart regeneration. Dev. Biol. *370*, 173–186.

González-Rosa, J.M., Burns, C.E., and Burns, C.G. (2017). Zebrafish heart regeneration: 15 years of discoveries. Regeneration (Oxf.) *4*, 105–123.

González-Rosa, J.M., Sharpe, M., Field, D., Soonpaa, M.H., Field, L.J., Burns, C.E., and Burns, C.G. (2018). Myocardial polyploidization creates a barrier to heart regeneration in zebrafish. Dev. Cell *44*, 433–446.e7.

Grego-Bessa, J., Luna-Zurita, L., del Monte, G., Bolós, V., Melgar, P., Arandilla, A., Garratt, A.N., Zang, H., Mukouyama, Y.-S., Chen, H., et al. (2007). Notch signaling is essential for ventricular chamber development. Dev. Cell *12*, 415–429.

Gu, B., Watanabe, K., Sun, P., Fallahi, M., and Dai, X. (2013). Chromatin effector Pygo2 mediates Wnt-notch crosstalk to suppress luminal/alveolar potential of mammary stem and basal cells. Cell Stem Cell *13*, 48–61.

Han, P., Bloomekatz, J., Ren, J., Zhang, R., Grinstein, J.D., Zhao, L., Burns, C.G., Burns, C.E., Anderson, R.M., and Chi, N.C. (2016). Coordinating cardiomyocyte interactions to direct ventricular chamber morphogenesis. Nature *534*, 700–704.

Harrison, M.R.M., Bussmann, J., Huang, Y., Zhao, L., Osorio, A., Burns, C.G., Burns, C.E., Sucov, H.M., Siekmann, A.F., and Lien, C.-L. (2015). Chemokine-guided angiogenesis directs coronary vasculature formation in zebrafish. Dev. Cell *33*, 442–454.

Heallen, T., Zhang, M., Wang, J., Bonilla-Claudio, M., Klysik, E., Johnson, R.L., and Martin, J.F. (2011). Hippo pathway inhibits Wnt signaling to restrain cardiomyocyte proliferation and heart size. Science *332*, 458–461.

Hsieh, J.C., Kodjabachian, L., Rebbert, M.L., Rattner, A., Smallwood, P.M., Samos, C.H., Nusse, R., Dawid, I.B., and Nathans, J. (1999). A new secreted protein that binds to Wnt proteins and inhibits their activities. Nature *398*, 431–436.

Huang, S.-M.A., Mishina, Y.M., Liu, S., Cheung, A., Stegmeier, F., Michaud, G.A., Charlat, O., Wiellette, E., Zhang, Y., Wiessner, S., et al. (2009). Tankyrase inhibition stabilizes axin and antagonizes Wnt signalling. Nature *461*, 614–620.

Huang, M., Chang, A., Choi, M., Zhou, D., Anania, F.A., and Shin, C.H. (2014). Antagonistic interaction between Wnt and Notch activity modulates the regenerative capacity of a zebrafish fibrotic liver model. Hepatology *60*, 1753–1766.

Jin, S.-W., Beis, D., Mitchell, T., Chen, J.-N., and Stainier, D.Y.R. (2005). Cellular and molecular analyses of vascular tube and lumen formation in zebrafish. Development *132*, 5199–5209.

Jopling, C., Sleep, E., Raya, M., Martí, M., Raya, A., and Izpisúa Belmonte, J.C. (2010). Zebrafish heart regeneration occurs by cardiomyocyte dedifferentiation and proliferation. Nature *464*, 606–609.

Jung, H.M., Isogai, S., Kamei, M., Castranova, D., Gore, A.V., and Weinstein, B.M. (2016). Imaging blood vessels and lymphatic vessels in the zebrafish. Methods Cell Biol. *133*, 69–103.

Kakugawa, S., Langton, P.F., Zebisch, M., Howell, S., Chang, T.-H., Liu, Y., Feizi, T., Bineva, G., O'Reilly, N., Snijders, A.P., et al. (2015). Notum deacylates Wnt proteins to suppress signalling activity. Nature *519*, 187–192.

Kikuchi, K., Holdway, J.E., Werdich, A.A., Anderson, R.M., Fang, Y., Egnaczyk, G.F., Evans, T., Macrae, C.A., Stainier, D.Y.R., and Poss, K.D. (2010). Primary contribution to zebrafish heart regeneration by gata4(+) cardiomyocytes. Nature *464*, 601–605.

Kikuchi, K., Holdway, J.E., Major, R.J., Blum, N., Dahn, R.D., Begemann, G., and Poss, K.D. (2011). Retinoic acid production by endocardium and epicardium is an injury response essential for zebrafish heart regeneration. Dev. Cell *20*, 397–404.

Kwan, K.M., Fujimoto, E., Grabher, C., Mangum, B.D., Hardy, M.E., Campbell, D.S., Parant, J.M., Yost, H.J., Kanki, J.P., and Chien, C.-B. (2007). The Tol2kit: a multisite gateway-based construction kit for Tol2 transposon transgenesis constructs. Dev. Dyn. *236*, 3088–3099.

Kwon, C., Cheng, P., King, I.N., Andersen, P., Shenje, L., Nigam, V., and Srivastava, D. (2011). Notch post-translationally regulates β-catenin protein in stem and progenitor cells. Nat. Cell Biol. *13*, 1244–1251.

Lai, S.-L., Marín-Juez, R., Moura, P.L., Kuenne, C., Lai, J.K.H., Tsedeke, A.T., Guenther, S., Looso, M., and Stainier, D.Y. (2017). Reciprocal analyses in zebrafish and medaka reveal that harnessing the immune response promotes cardiac regeneration. eLife *6*, e25605.

Li, W., Wu, J., Yang, J., Sun, S., Chai, R., Chen, Z.-Y., and Li, H. (2015). Notch inhibition induces mitotically generated hair cells in mammalian cochleae via activating the Wnt pathway. Proc. Natl. Acad. Sci. USA *112*, 166–171.

Luxán, G., Casanova, J.C., Martínez-Poveda, B., Prados, B., D'Amato, G., MacGrogan, D., González-Rajal, A., Dobarro, D., Torroja, C., Martinez, F., et al. (2013). Mutations in the NOTCH pathway regulator MIB1 cause left ventricular noncompaction cardiomyopathy. Nat. Med. *19*, 193–201.

Luxán, G., D'Amato, G., MacGrogan, D., and de la Pompa, J.L. (2016). Endocardial Notch signaling in cardiac development and disease. Circ. Res. *118*, e1–e18.

McCurley, A.T., and Callard, G.V. (2008). Characterization of housekeeping genes in zebrafish: male-female differences and effects of tissue type, developmental stage and chemical treatment. BMC Mol. Biol. *9*, 102.

Metsalu, T., and Vilo, J. (2015). ClustVis: a web tool for visualizing clustering of multivariate data using principal component analysis and heatmap. Nucleic Acids Res. *43* (*W1*), W566–W570.

Mi, H., Huang, X., Muruganujan, A., Tang, H., Mills, C., Kang, D., and Thomas, P.D. (2017). PANTHER version 11: expanded annotation data from Gene Ontology and Reactome pathways, and data analysis tool enhancements. Nucleic Acids Res. *45* (*D1*), D183–D189.

Moro, E., Ozhan-Kizil, G., Mongera, A., Beis, D., Wierzbicki, C., Young, R.M., Bournele, D., Domenichini, A., Valdivia, L.E., Lum, L., et al. (2012). In vivo Wnt signaling tracing through a transgenic biosensor fish reveals novel activity domains. Dev. Biol. *366*, 327–340.

Münch, J., Grivas, D., González-Rajal, Á., Torregrosa-Carrión, R., and de la Pompa, J.L. (2017). Notch signalling restricts inflammation and *serpine1* expression in the dynamic endocardium of the regenerating zebrafish heart. Development *144*, 1425–1440.

Nery, L.R., Eltz, N.S., Martins, L., Guerim, L.D., Pereira, T.C., Bogo, M.R., and Vianna, M.R.M. (2014). Sustained behavioral effects of lithium exposure during early development in zebrafish: involvement of the Wnt-β-catenin signaling pathway. Prog. Neuropsychopharmacol. Biol. Psychiatry *55*, 101–108.

Nicolas, M., Wolfer, A., Raj, K., Kummer, J.A., Mill, P., van Noort, M., Hui, C.-C., Clevers, H., Dotto, G.P., and Radtke, F. (2003). Notch1 functions as a tumor suppressor in mouse skin. Nat. Genet. *33*, 416–421.

Ozhan, G., and Weidinger, G. (2015). Wnt/β-catenin signaling in heart regeneration. Cell Regen. (Lond.) *4*, 3.

Polychronopoulos, P., Magiatis, P., Skaltsounis, A.-L., Myrianthopoulos, V., Mikros, E., Tarricone, A., Musacchio, A., Roe, S.M., Pearl, L., Leost, M., et al. (2004). Structural basis for the synthesis of indirubins as potent and selective inhibitors of glycogen synthase kinase-3 and cyclin-dependent kinases. J. Med. Chem. *47*, 935–946.

Porrello, E.R., Mahmoud, A.I., Simpson, E., Hill, J.A., Richardson, J.A., Olson, E.N., and Sadek, H.A. (2011). Transient regenerative potential of the neonatal mouse heart. Science *331*, 1078–1080.

Poss, K.D., Wilson, L.G., and Keating, M.T. (2002). Heart regeneration in zebrafish. Science *298*, 2188–2190.

Raya, A., Koth, C.M., Büscher, D., Kawakami, Y., Itoh, T., Raya, R.M., Sternik, G., Tsai, H.-J., Rodríguez-Esteban, C., and Izpisúa-Belmonte, J.C. (2003). Activation of Notch signaling pathway precedes heart regeneration in zebrafish. Proc. Natl. Acad. Sci. USA *100* (*Suppl 1*), 11889–11895.

Russell, J.L., Goetsch, S.C., Gaiano, N.R., Hill, J.A., Olson, E.N., and Schneider, J.W. (2011). A dynamic notch injury response activates epicardium and contributes to fibrosis repair. Circ. Res. *108*, 51–59.

Sato, N., Meijer, L., Skaltsounis, L., Greengard, P., and Brivanlou, A.H. (2004). Maintenance of pluripotency in human and mouse embryonic stem cells through activation of Wnt signaling by a pharmacological GSK-3-specific inhibitor. Nat. Med. *10*, 55–63.

Schnabel, K., Wu, C.-C., Kurth, T., and Weidinger, G. (2011). Regeneration of cryoinjury induced necrotic heart lesions in zebrafish is associated with epicardial activation and cardiomyocyte proliferation. PLoS One *6*, e18503.

Stoick-Cooper, C.L., Weidinger, G., Riehle, K.J., Hubbert, C., Major, M.B., Fausto, N., and Moon, R.T. (2007). Distinct Wnt signaling pathways have opposing roles in appendage regeneration. Development *134*, 479–489.

Tian, H., Biehs, B., Chiu, C., Siebel, C.W., Wu, Y., Costa, M., de Sauvage, F.J., and Klein, O.D. (2015). Opposing activities of Notch and Wnt signaling regulate intestinal stem cells and gut homeostasis. Cell Rep. *11*, 33–42.

Tseng, A.-S., Engel, F.B., and Keating, M.T. (2006). The GSK-3 inhibitor BIO promotes proliferation in mammalian cardiomyocytes. Chem. Biol. *13*, 957–963.

VanDusen, N.J., Casanovas, J., Vincentz, J.W., Firulli, B.A., Osterwalder, M., Lopez-Rios, J., Zeller, R., Zhou, B., Grego-Bessa, J., De La Pompa, J.L., et al. (2014). Hand2 is an essential regulator for two Notch-dependent functions within the embryonic endocardium. Cell Rep. *9*, 2071–2083.

Yang, D., Fu, W., Li, L., Xia, X., Liao, Q., Yue, R., Chen, H., Chen, X., An, S., Zeng, C., and Wang, W.E. (2017). Therapeutic effect of a novel Wnt pathway inhibitor on cardiac regeneration after myocardial infarction. Clin. Sci. (Lond.) *131*, 2919–2932.

Ye, B., Hou, N., Xiao, L., Xu, Y., Boyer, J., Xu, H., and Li, F. (2015). APC controls asymmetric Wnt/β-catenin signaling and cardiomyocyte proliferation gradient in the heart. J. Mol. Cell. Cardiol. *89* (*Pt B*), 287–296.

Zaucker, A., Mercurio, S., Sternheim, N., Talbot, W.S., and Marlow, F.L. (2013). notch3 is essential for oligodendrocyte development and vascular integrity in zebrafish. Dis. Model. Mech. *6*, 1246–1259.

Zhang, R., Han, P., Yang, H., Ouyang, K., Lee, D., Lin, Y.-F., Ocorr, K., Kang, G., Chen, J., Stainier, D.Y.R., et al. (2013). In vivo cardiac reprogramming contributes to zebrafish heart regeneration. Nature *498*, 497–501.

Zhao, L., Borikova, A.L., Ben-Yair, R., Guner-Ataman, B., MacRae, C.A., Lee, R.T., Burns, C.G., and Burns, C.E. (2014). Notch signaling regulates cardiomyocyte proliferation during zebrafish heart regeneration. Proc. Natl. Acad. Sci. USA *111*, 1403–1408.

STAR★METHODS

KEY RESOURCES TABLE

REAGENT or RESOURCE	SOURCE	IDENTIFIER
Antibodies		
Mouse monoclonal MF20	Deposited to the Developmental Studies Hybridoma Bank by Fischman, D.A.	DSHB Cat# MF20; RRID: AB_2147781
Mouse monoclonal anti-mCherry	Abcam	Cat# ab125096; RRID: AB_11133266
Rabbit polyclonal anti-GFP	Abcam	Cat# ab290; RRID: AB_303395
Chicken polyclonal anti-GFP	Abcam	Cat# ab13970; RRID: AB_300798
Rabbit polyclonal anti-Wif1	GeneTex	Cat# GTX16429;
Rabbit polyclonal anti-Notum	GeneTex	Cat# GTX85260; RRID: AB_10722930
Rabbit polyclonal anti-Mef2	Santa Cruz Biotechnology	Cat# sc-313; RRID: AB_631920
Mouse monoclonal anti-PCNA	Sigma-Aldrich	Cat# WH0005111M2; RRID: AB_1842895
Mouse monoclonal anti-pan Cytokeratin	Abcam	Cat# ab86734; RRID: AB_10674321
Mouse monoclonal anti- Collagen, Type I pro-peptide	Deposited to the Developmental Studies Hybridoma Bank by Furthmayr, H.	DSHB Cat# SP1.D8; RRID: AB_528438
Goat anti-Mouse IgG (H+L) Cross-Absorbed Secondary Antibody, Alexa Fluor 488	Thermo Fisher Scientific	Cat# A-11029; RRID: AB_2534088
Goat anti-Rabbit IgG (H+L) Cross-Absorbed Secondary Antibody, Alexa Fluor 488	Thermo Fisher Scientific	Cat# A-11008; RRID: AB_143165
Goat anti-Mouse IgG2b Cross-Absorbed Secondary Antibody, Alexa Fluor 546	Thermo Fisher Scientific	Cat# A-21143; RRID: AB_2535779
Goat anti-Mouse IgG (H+L) Cross-Absorbed Secondary Antibody, Alexa Fluor 555	Thermo Fisher Scientific	Cat# A-21424; RRID: AB_141780
Goat anti-Mouse IgG1 Cross-Absorbed Secondary Antibody, Alexa Fluor 568	Thermo Fisher Scientific	Cat# A-21124; RRID: AB_2535766
Goat anti-Rabbit IgG (H+L) Cross-Adsorbed Secondary Antibody, Alexa Fluor 568	Thermo Fisher Scientific	Cat# A-11036; RRID: AB_10563566
Goat anti-Chick IgY (H+L) Cross-Absorbed Secondary Antibody, Alexa Fluor 633	Thermo Fisher Scientific	Cat# A-21103; RRID: AB_2535756
Goat anti-Mouse IgG2b Cross-Absorbed Secondary Antibody, Alexa Fluor 647	Thermo Fisher Scientific	Cat# A-21242; RRID: AB_2535811
Chemicals, Peptides, and Recombinant Proteins		
Ethyl-Aminobenzoate methanesulfonate salt (MS-222, Tricaine)	Sigma-Aldrich	Cat# A5040
Nitro-Blue Tetrazolium Chloride (NBT)	Promega	Cat# S380C
5-Bromo-4-Chloro-3-Indolyphosposphate p-Toluidine.(BCIP)	Promega	Cat# S381C
4-Hydroxytamoxifen	Sigma-Aldrich	Cat# H7904
Aniline Blue	Sigma-Aldrich	Cat# 415049
Orange G	Sigma-Aldrich	Cat# O3756
Acid Fuchsin	Sigma-Aldrich	Cat# F8129
Trizol	Invitrogen	Cat# 15596-026
(2′Z,3′E)-6-Bromoindirubin-3′-oxime (BIO)	Sigma-Aldrich	Cat# B1686
IWR-1-endo (IWR)	Sigma-Aldrich	Cat# 681669
Critical Commercial Assays		
DIG RNA Labeling Kit (SP6/T7)	Roche	Cat# 11175025910
TSA-plus DNP system	PerkinElmer	Cat# NEL746A

(*Continued on next page*)

Continued		
REAGENT or RESOURCE	SOURCE	IDENTIFIER
RNeasy Plus Micro Kit	QIAGEN	Cat# 74034
SuperScript III First-Strand Synthesis System	Thermo Fisher Scientific	Cat# 18080051
Fast SYBER Green PCR Master Mix	Thermo Fisher Scientific	Cat# 4385612
Zero Blunt TOPO PCR Cloning Kit	Invitrogen	Cat# 450245
Deposited Data		
RNA Sequencing Data	This paper	GSE107228
Experimental Models: Organisms/Strains		
Zebrafish: *Tg(hsp70l:DN-MAML)^{fb14}*	Zhao et al., 2014	ZFIN: ZDB-ALT-140618-1
Zebrafish: *Tg(kdrl:CreERT2)^{fb13}*	Zhao et al., 2014	ZFIN: ZDB-ALT-140522-6
Zebrafish: *Tg(kdrl:mCherry-ras)^{s896}*	Chi et al., 2008	ZFIN: ZDB-ALT-081212-4
Zebrafish: *Tg(hsp70l:loxPmKate2STOPloxPDN-MAML-GFP)^{fb24}*	This paper	N/A
Zebrafish: *Tg(7XTCF-Xla.Siam:GFP)^{ia4}*	Moro et al., 2012	ZFIN: ZDB-ALT-110113-1
Oligonucleotides		
See Table S2		N/A
Recombinant DNA		
p5E-*hsp70l*	Kwan et al., 2007	N/A
pME-*loxP-mKate2-Stop-loxP*	Han et al., 2016	N/A
p3E-*DN-MAML-GFP*	Han et al., 2016	N/A
pDestTol2pA2	Kwan et al., 2007	N/A
pDestTol2pA2-*hsp70l-loxPmKate2STOPloxPDN-MAML-GFP*	This paper	N/A
TOPO-*wif1*	This paper	N/A
TOPO-*notum1b*	This paper	N/A
Software and Algorithms		
NIS-Elements	Nikon Instruments	RRID: SCR_014329
Fiji/ImageJ	NIH	RRID: SCR_002285
GraphPad Prism 6	GraphPad Software	RRID: SCR_002798
RStudio	RStudio	https://www.rstudio.com/RRID: SCR_000432
Microsoft Excel	Microsoft	RRID: SCR_016137
ClustVis	Metsalu and Vilo. 2015	https://biit.cs.ut.ee/clustvis
PANTHER	Mi et al., 2017	http://www.pantherdb.org RRID: SCR_004869
Other		
4′,6-diamidino-2-phenylindole dihydrochloride (DAPI)	Invitrogen	Cat# D1306; RRID: AB_2629482
VECTASHIELD Antifade Mounting Medium	Vector Laboratories	Cat# H-1000; RRID: AB_2336789

CONTACT FOR REAGENT AND RESOURCE SHARING

Further information and requests for resources and reagents should be directed to and will be fulfilled by the Lead Contact, C. Geoffrey Burns (gburns@cvrc.mgh.harvard.edu).

EXPERIMENTAL MODEL AND SUBJECT DETAILS

Zebrafish embryos, larvae, and adults were grown and maintained according to standard protocols approved by the Massachusetts General Hospital Institutional Animal Care and Use Committee. Experimental and control animals of the same age, weight, underlying health, and sex ratios were analyzed in parallel. Zebrafish from 6 to 12 months of age were used for ventricular resection surgeries as described (Poss et al., 2002). Published strains used in this study include: wild-type AB; wild-type TuAB, *Tg(hsp70l:DN-MAML)^{fb14}* (published as fb10 in (Zhao et al., 2014) but changed to fb14 on ZFIN), *Tg(kdrl:CreERT2)^{fb13}* (Zhao et al., 2014), *Tg(7XTCF-Xla.Siam:GFP)^{ia4}* (Moro et al., 2012), and *Tg(kdrl:mCherry-ras)^{s896}* (Chi et al., 2008). Animal density was maintained at four fish per liter. Live embryos or adults were anesthetized in standard E3 media containing 0.4% tricaine (ethyl 3-aminobenzoate methanesulfonate salt; Sigma-Aldrich).

METHOD DETAILS

Construction of Tg(hsp70l:mKate2STOP^{flox}DN-MAML) Transgenic Line

To generate the *Tg(hsp70l:loxPmKate2STOPloxPDN-MAML-GFP)^{fb24}* conditional strain, abbreviated *Tg(hsp70l:mKate2STOP^{flox}DN-MAML)^{fb24}*, the transgene was engineered using Gateway technology (Life Sciences). An LR recombination reaction was conducted with *p5E-hsp70l* (Kwan et al., 2007), *pME-loxP-mKate2-Stop-loxP* (Han et al., 2016), *p3E-DN-MAML-GFP* (Han et al., 2016) entry vectors, and the *pDestTol2pA2* (Kwan et al., 2007) destination vector. This plasmid was injected into one-cell stage wild-type embryos together with *Tol2* transposase mRNA (Kwan et al., 2007). One founder was isolated and propagated.

4-HT treatments and heat shock induction

At 24 hour post-fertilization (hpf), embryos from heterozygous crosses between *Tg(kdrl:CreERT2)^{fb13}* and *Tg(hsp70l:mKate2STOP^{flox}DN-MAML)^{fb24}* were treated with E3 medium containing 5 μM 4-hydroxytamoxifen (4-HT; Sigma-Aldrich) for 24 hours. Control embryos were treated with E3 medium containing 0.05% vehicle (ethanol, EtOH) over the same time period. At 48 hpf, treated embryos were washed in E3 multiple times and those expressing the selectable cerulean lens marker from the *Tg(kdrl:CreERT2)^{fb13}* transgene were isolated. To learn which animals also carried the *Tg(hsp70l:mKate2STOP^{flox}DN-MAML)^{fb24}* transgene, the cerulean+ embryos were heat-shocked in a 38°C waterbath in 50ml Falcon tubes containing 25 mL E3 medium. After 45 minutes, embryos were transferred to a 28°C incubator for additional 4 hours. Embryos with EGFP expression throughout the blood vessels and endocardium were selected to propagate. In the EtOH-treated group, double transgenic embryos exhibited whole body red fluorescence that resulted from mKate2 expression without EGFP expression. Both control and experimental double transgenic strains were raised to adulthood for heart regeneration analyses.

Adult heat-shock treatments were performed as previously described (Zhao et al., 2014). Briefly, adult ventricles were injured by resection surgery and allowed to recover overnight in the aquatics facility. Animals were exposed to automated daily increases in temperature from 26°C to 38°C for one hour followed by gradual decreases in temperature to 26°C. In all experiments, hearts were harvested 5 hours after the final heat shock treatment.

Histological analysis and imaging

Cryosectioning was performed as previously described (Zhao et al., 2014). In brief, hearts were dissected and fixed in 4% paraformaldehyde (PFA) in PBS overnight at 4°C, washed in PBS, embedded in 1.2% (wt/vol) agarose in 5% (wt/vol) sucrose-PBS solution, equilibrated in 30% (wt/vol) sucrose-PBS solution overnight at 4°C, and frozen for cryosectioning on a Leica cryostat (CM3050S, Leica). 10 μm cryosections were used in all experiments.

Acid Fuchsin-Orange G (AFOG) staining was performed as described (Poss et al., 2002). *In situ* hybridization experiments for *wif1* and *notum1b* were carried out using Digoxygenin-labeled RNA probes with Tyramide Signal Amplification (TSA) plus DIG Reagent kit (PerkinElmer) according to the manufacturer's instructions. Fragments of *wif1* (1.2 kb) and *notum1b* (0.6 kb) were cloned from a 24-72 hpf zebrafish embryonic cDNA library using oligos as detailed in Table S2.

For immunofluorescence, cryosections were immersed in boiling citric acid buffer (10mM) for antigen retrieval. Following PBS washes, sections were permeabilized with 0.5% Triton X-100 in PBS, blocked in blocking buffer (5% BSA, 5% goat serum, 20mM $MgCl_2$) for 1 h at room temperature, and incubated with primary antibodies in PBS containing 5% BSA overnight at 4°C. Sections were incubated in secondary antibodies at room temperature for 1 h and mounted with Vectashield medium (Vector Laboratories).

Cardiomyocyte proliferation indices were quantified by manually counting Mef2+ and Mef2+/PCNA$^+$ cells in injury regions. To determine the proliferation index of each heart, data from 4-6 sections with the largest ventricular wound area were averaged.

Primary antibodies used in this study include anti-mCherry (mouse, 1:200; Abcam); anti-EGFP (rabbit, 1:100; Abcam), anti-myosin heavy chain monoclonal antibody (MF20, mouse, 1:50; Developmental Studies Hybridoma Bank), anti-Wif1 (rabbit, 1:100, GeneTex), anti-Notum (rabbit, 1:100, GeneTex), anti-Mef2 (rabbit, 1:50; Santa Cruz Biotechnology), anti-PCNA (mouse, 1:200; Sigma-Aldrich), anti-GFP (chicken, 1:800, Abcam), anti-pan Cytokeratin (mouse, 1:100, Abcam) and anti-Collagen Type I, SP1.D8 (mouse, 1:20, Developmental Hybridoma Bank). Secondary antibodies (1:200; Life Technologies) used in this study include Alexa Fluor 488 goat anti-mouse IgG (H+L), Alexa Fluor 488 goat anti-rabbit IgG (H+L), Alexa Fluor 546 goat anti-mouse IgG2b, Alexa Fluor 633 goat anti-chicken IgY(H+L), Alexa Fluor 555 goat anti-mouse IgG (H+L), Alexa Fluor 568 goat anti-mouse IgG1, Alexa Fluor 568 goat anti-rabbit IgG (H+L), Alexa Fluor 647 goat anti-mouse IgG2b.

AFOG staining and *in situ* hybridization images were captured using a Nikon Eclipse 80i compound microscope (Nikon) and *Excelis* AU600HDS HD Camera & Monitor System (Accu-Scope Inc. Commack, NY). Sections of PCNA/Mef2 antibody staining were imaged using a Nikon Eclipse 80i compound microscope with 20x objective and a QImaging Retiga 2000R CCD camera (QImaging). Whole heart bright field and fluorescence images were captures using a Nikon Eclipse 80i compound microscope with 4x objective and a QImaging Retiga 2000R CCD camera (QImaging). Other immunofluorescence images were taken using a Nikon A1 (Adaptor Set with Eclipse Ti) confocal microscope (Nikon).

Quantification of Scar Tissue in Regenerated Hearts

Quantification of scar area in regenerated hearts at 30 dpa was performed as described previously (Chablais et al., 2011; González-Rosa et al., 2018; Schnabel et al., 2011). Serial sections of AFOG-stained hearts were imaged using a Nikon 80i compound microscope (Nikon) with a 4x objective and *Excelis* AU600HDS HD Camera & Monitor System (Accu-Scope Inc. Commack, NY). Whole ventricular area and scar area [fibrin (red) + collagen (blue)] were measured using Fiji software. The scar area was normalized to the whole ventricular area to calculate the percentage of the scar size for each heart. Scar percentage data were collected for 6-10 sections per heart and averaged to generate each data point.

Alkaline phosphatase staining

Alkaline phosphatase staining was performed as previously described (Jung et al., 2016; Lai et al., 2017) with modifications. Hearts were fixed in 4% paraformaldehyde (PFA) in PBS for 1 h at room temperature. Prior to washing in PBS (three times for 10 each), the atria were removed with forceps. Hearts were then equilibrated in alkaline buffer (100 mM Tris, pH 9.5, 50 mM MgCl2, 100 mM NaCl, 0.1% Tween 20 – 2 washes, 5 min each) and stained with BCIP (3.5 μl/ml) and NBT (4.5 μl/ml) in alkaline buffer in the dark. To stop the reaction, hearts were washed in PBS three times and fixed and stored in 4% PFA at 4°C. Hearts were imaged in 100% glycerol. Images were acquired with a Leica MZ12 microscope (Leica) and SPOT Insight QE CCD camera (SPOT Imaging).

Quantification of vessel leakiness

Adults were anesthetized and imaged with a Leica MZ12 microscope (Leica) and SPOT Insight QE CCD camera (SPOT Imaging). Bleeding in each area of every fish was calculated as described previously (Zaucker et al., 2013).

RNA sequencing and transcriptomic analysis

RNA sequencing of 5 dpa ventricles from *Tg(hsp70l:DN-MAML^{ubi})^{fb14}* [abbreviated *Tg(DN-MAML)^{ubi}*] and non-transgenic wild-type siblings was performed. Specifically, adult ventricles were amputated and exposed to daily heat shocking until 5 dpa. The apical portions of 5 resected ventricles were harvested and pooled for each sample approximately 6 hours after the final heat shock. For both experimental groups, 3 samples were collected. Total RNA was extracted using RNeasy Plus Micro Kit (QIAGEN) as per the manufacturer's instructions. cDNA libraries were prepared and sequenced at the PCPGM on an Illumina HiSeq 2000 sequencer. Differentially expressed genes ($p < 0.0001$) were selected for transcriptomic analysis (see Table S1). A heatmap was generated by ClustVis (Metsalu and Vilo, 2015) online tools (https://biit.cs.ut.ee/clustvis/). Gene Ontology enrichment and clustering calculation were analyzed using PANTHER (Mi et al., 2017) (http://www.pantherdb.org/). The accession number for the raw RNA-Sequencing data reported in this paper has been deposited in NCBI Gene Expression Omnibus Database: GSE107228.

Small molecule treatments

To detect potential changes in the expression of Wnt target genes by quantitative PCR, the GSK-3 inhibitor 6-Bromoindirubin-3-oxime (BIO, Sigma-Aldrich) or the Wnt antagonist IWR-1-endo (IWR, Sigma-Aldrich) was dissolved in DMSO to a final concentration of 10 mM and wild-type adult zebrafish were injected intraperitonealy twice in a 24 hour period with 25 μL of IWR (10 μM in PBS), BIO (10 μM in PBS), or DMSO (0.1% in PBS). Ventricles were dissected 5 hours after the second injection for quantitative PCR as described below.

To test whether modulation of Wnt signaling affects myocardial proliferation and regenerative capacity, ventricles from wild-type animals were amputated and allowed to recover for 2 days in the aquatics facility. These animals were injected intraperitoneally with 25 μL of IWR (10 μM in PBS), BIO (10 μM in PBS), or DMSO (0.1% in PBS). The injection was performed at 5 dpa and 6 dpa for CM proliferation analysis at 7 dpa. For 30 dpa regeneration analysis, drugs were injected once every two days from 2 dpa throughout 30 dpa.

For rescue of myocardial proliferation in Notch-inhibited animals, *Tg(kdrl:CreERT2)^{fb13};Tg(hsp70l:DN-MAML^{flox})^{fb24}* embryos were treated with 4-HT or EtOH as previously described during embryogenesis and raised to adulthood. Following ventricular amputation, the fish were heat shocked daily from 1 dpa to 7 dpa. On days 6 and 7, the fish were injected intraperitoneally three hours after heat shock with 25 μL of IWR (10 μM in PBS) or DMSO (0.1% in PBS).

Quantitative PCR

Apical ventricular wound regions, uninjured ventricular spared regions, or whole ventricles of 3-5 hearts were collected in TRIzol for each biological replicate. Three biological replicates were analyzed per experimental group. Total RNA was extracted from each sample using Trizol reagent (Invitrogen) and chloroform (Sigma-Aldrich), and reverse transcription carried out using the Super Script III first-Strand Synthesis System (Life Technologies) according to the manufacturer's protocol. Quantitative PCR was performed in triplicate with the Applied Biosystems 7500 Fast or Quant Studio3 Real-Time PCR System (Applied Biosystems, Thermo Fisher Scientific) with Fast SYBER Green PCR Master Mix (Applied Biosystems, Thermo Fisher Scientific). Threshold cycles (Cts) for selected transcripts were normalized to *ef1alpha* (McCurley and Callard, 2008) prior to calculating fold differences in gene expression between experimental groups. A complete list of the primers used in this study is provided in Table S2.

QUANTIFICATION AND STATISTICAL ANALYSIS

Sample sizes, statistical tests, and *P value*s are indicated in the figures or figure legends. The experiments were not randomized, and the investigators were not blinded to allocation during experiments and outcome assessment. All statistical values are displayed as mean ± standard deviation. An unpaired two-tailed t test with unequal variance using Microsoft Excel (Microsoft) was used to assess all comparisons. Statistical significance was assigned at $p < 0.05$. Scatterplots in Figures 1K, 3K and 4F were generated using GraphPad Prism 6. Boxplots in Figures S1U and S6AA and volcano plot in Figure S3A were generated using RStudio.

DATA AND SOFTWARE AVAILABILITY

The RNA-seq data reported in this study is available under accession number GSE107228 at the Gene Expression Omnibus.